Liver Iron Quantification with MR Imaging: A Primer for Radiologists[1]

Roxanne Labranche, MD
Guillaume Gilbert, PhD
Milena Cerny, MD
Kim-Nhien Vu, MD
Denis Soulières, MD, MSc
Damien Olivié, MD
Jean-Sébastien Billiard, MD, FRCPC
Takeshi Yokoo, MD, PhD
An Tang, MD, MSc, FRCPC

Abbreviations: GRE = gradient-echo, ROI = region of interest, TE = echo time

RadioGraphics 2018; 38:392–412

https://doi.org/10.1148/rg.2018170079

Content Codes: GI MR

[1]From the Department of Radiology (R.L., G.G., M.C., K.N.V., D.O., J.S.B., A.T.) and Service of Hemato-oncology, Department of Medicine (D.S.), Centre Hospitalier de l'Université de Montréal, 1000 rue Saint-Denis, Montréal, QC, Canada H2X 0C2; MR Clinical Science, Philips Healthcare Canada, Markham, ON, Canada (G.G.); Department of Radiology and Advanced Imaging Research Center, University of Texas Southwestern Medical Center, Dallas, Tex (T.Y.); and Centre de Recherche du Centre Hospitalier de l'Université de Montréal, Montréal, QC, Canada (A.T.). Recipient of a Certificate of Merit award for an education exhibit at the 2016 RSNA Annual Meeting. Received April 3, 2017; revision requested July 7 and received July 31; accepted August 10. For this journal-based SA-CME activity, the authors, editor, and reviewers have disclosed no relevant relationships. **Address correspondence to** A.T. (e-mail: *an.tang@umontreal.ca*).

Supported by the Institute of Nutrition, Metabolism, and Diabetes, Canadian Institutes of Health Research (Operating Grants 273738 and 301520). A.T. supported by the Fonds de Recherche du Québec en Santé and Fondation de l'Association des Radiologistes du Québec (Clinical Research Scholarship–Junior 1 Salary Award 26993).

Iron overload is a systemic disorder and is either primary (genetic) or secondary (exogenous iron administration). Primary iron overload is most commonly associated with hereditary hemochromatosis and secondary iron overload with ineffective erythropoiesis (predominantly caused by β-thalassemia major and sickle cell disease) that requires long-term transfusion therapy, leading to transfusional hemosiderosis. Iron overload may lead to liver cirrhosis and hepatocellular carcinoma, in addition to cardiac and endocrine complications. The liver is one of the main iron storage organs and the first to show iron overload. Therefore, detection and quantification of liver iron overload are critical to initiate treatment and prevent complications. Liver biopsy was the historical reference standard for detection and quantification of liver iron content. Magnetic resonance (MR) imaging is now commonly used for liver iron quantification, including assessment of distribution, detection, grading, and monitoring of treatment response in iron overload. Several MR imaging techniques have been developed for iron quantification, each with advantages and limitations. The liver-to-muscle signal intensity ratio technique is simple and widely available; however, it assumes that the reference tissue is normal. Transverse magnetization (also known as R2) relaxometry is validated but is prone to respiratory motion artifacts due to a long acquisition time, is presently available only for 1.5-T imaging, and requires additional cost and delay for off-line analysis. The R2* technique has fast acquisition time, demonstrates a wide range of liver iron content, and is available for 1.5-T and 3.0-T imaging but requires additional postprocessing software. Quantitative susceptibility mapping has the highest sensitivity for detecting iron deposition; however, it is still investigational, and the correlation with liver iron content is not yet established.

SA-CME LEARNING OBJECTIVES

After completing this journal-based SA-CME activity, participants will be able to:

- Describe the distribution and potential complications of iron overload.
- Discuss the advantages and limitations of the liver-to-muscle signal intensity ratio technique, R2 and R2* relaxometry, and quantitative susceptibility mapping for quantification of liver iron.
- List the benefits of MR imaging–based liver iron detection, quantification, monitoring, and assessment of treatment response.

See www.rsna.org/education/search/RG.

TEACHING POINTS

- Noninvasive quantification of iron with MR imaging is now considered the standard of care in diagnosis and monitoring of iron overload diseases.
- Although iron overload can be seen in many organs, the liver is the main iron storage organ, the first to show iron overload, and the only one to show a linear relationship between its iron concentration and total body iron. Therefore, MR imaging for quantification of liver iron provides a good estimate of the degree of iron overload and allows prediction of the risk of complications.
- Detection of iron overload is important owing to the risk of complications such as myocardial disease, liver cirrhosis, and increased risk of hepatocellular carcinoma development in untreated patients.
- Annual liver iron quantification with MR imaging is recommended for patients undergoing long-term transfusion, starting at the age of initial diagnosis.
- Preliminary results suggest that ultrashort-TE sequences may represent a viable replacement for or alternative to conventional GRE sequences for R2* estimation, for both low and high iron overload.

Introduction

Iron overload is a systemic disorder characterized by a high level of plasma iron and accumulation of iron in parenchymal cells in the form of ferritin and hemosiderin. The liver is the main iron storage organ (in hepatocytes and Kupffer cells) and the first to show iron overload (1).

Oral intake of iron in a normal diet is approximately 10–20 mg/d, of which only 1–2 mg is absorbed in the proximal duodenum by the ferroportin transporters, which are regulated by the protein hepcidin (1,2). Plasma iron is then transported in the bloodstream by the protein transferrin (Fig 1).

In the event of iron overload, the transferrin saturation can exceed 45% (normal range, 20%–45%), at which point non–transferrin-bound iron is created, which has a high affinity for parenchymal cells, especially hepatocytes (3,4). Eventually, if the transferrin saturation exceeds 75%, a new form of non–transferrin-bound iron is produced—labile plasma iron—which has the potential to produce toxic reactive radicals (5). When not immediately needed, iron is stored in its ferric form (Fe^{3+}) within ferritin and eventually within hemosiderin if ferritin storage is saturated (1,6) (Table 1).

Iron-deposition diseases can be classified into two main categories: primary iron overload caused by genetic diseases and secondary iron overload caused by exogenous iron (Table 2). Primary iron overload is most often associated with hereditary hemochromatosis, which is caused by mutations in the "high iron Fe" *(HFE)* gene. The homozygote form is the most common variant and affects 2% of those of northern European descendancy (7). This leads to decreased production of hepcidin, the protein responsible for regulation of iron absorption in the enterocytes (1,2). Other genetic diseases, such as hereditary aceruloplasminemia, ferroportin diseases, and hereditary atransferrinemia, are rare (1).

Secondary iron overload is mostly associated with multiple red blood cell transfusions in patients with red blood cell disorders, including β-thalassemia major, sickle cell disease, myelodysplasic syndromes, Blackfan-Diamond anemia, and aplastic anemia (8). Moreover, diseases linked with abnormal hemoglobins or thalassemia also interfere with expression of hepcidin, therefore also increasing iron overload by increased intestinal absorption. This is well demonstrated in thalassemia intermedia, in which patients can have iron overload without transfusion. Less commonly, parenteral iron administration or oral iron supplementation may also cause iron overload (2,9), such as in those with end-stage renal disease.

Clinically significant variants of hemoglobinopathies (including hemoglobin S, hemoglobin C, hemoglobin E, hemoglobin D, β-thalassemia, and α^0 thalassemia) are carried by 18% of the population in Africa; α-thalassemia variants are most common in Southeast Asia, Africa, and the Eastern Mediterranean region, where they are carried by 45%, 41%, and 19% of the population, respectively (10). There is a strong correlation between sickle cell disease and thalassemia in malaria-endemic regions because abnormal red blood cells offer some level of protection against malaria (11,12). The high prevalence of iron overload in these regions is a major public health concern.

Patients with hemochromatosis or transfusional hemosiderosis have higher transferrin and ferritin levels and accumulation of free iron, particularly in the hepatocytes. Iron overload in the liver generates the release of reactive oxygen species (5), causing toxic effects on the cellular membrane and nuclei of the hepatocytes. Detection and grading of iron overload are critical because not treating or poorly treating it may lead to organ dysfunction and damage through oxidative cytotoxicity (1). Iron overload in the heart can cause cardiomyopathy, which may result in decreased left ventricular ejection fraction, congestive heart failure, and ventricular arrhythmias; iron in the liver may lead to cirrhosis with increased risk of developing hepatocellular carcinoma and end-stage liver disease requiring transplant; iron in endocrine organs such as the pituitary gland may cause growth failure and in the pancreas may cause type 2 diabetes (13,14).

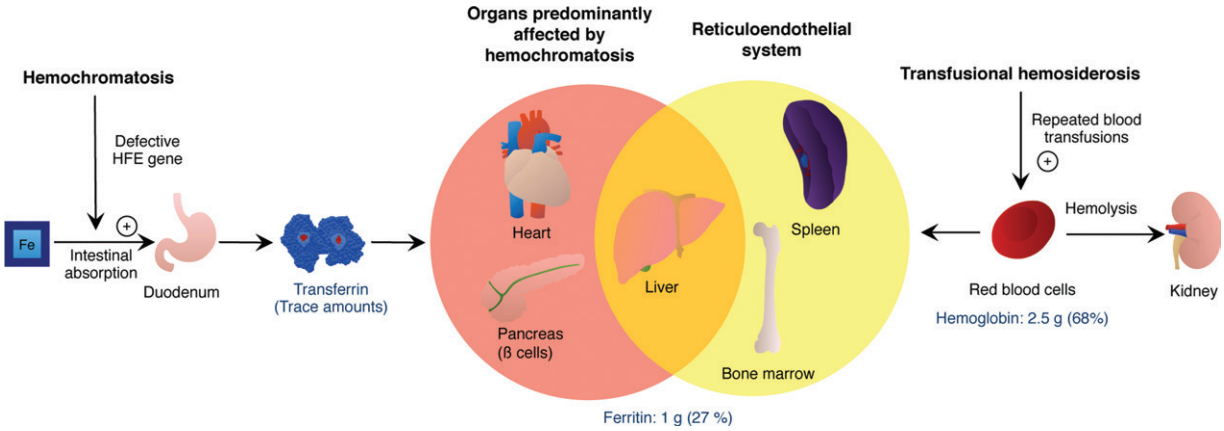

Figure 1. Iron *(Fe)* metabolism. Absorption of oral iron intake occurs in the duodenum, near the gastroduodenal junction. Hemochromatosis is caused by a defect in the *HFE* gene. In hemochromatosis, iron overload is predominantly distributed in the hepatocytes in the liver and eventually in other organs, predominantly in the β cells in the pancreas and in the heart. Hemosiderosis is caused by repeated blood transfusions, typically in sickle cell disease and β-thalassemia major. In hemosiderosis, iron overload is concentrated in the reticuloendothelial system, predominantly the spleen, bone marrow, and Kupffer cells in the liver. Hemolysis in hemolytic anemias can lead to iron accumulation in the proximal convoluted tubules of the kidneys.

Table 1: Molecules for Transport or Storage of Iron

Molecules	Amount	Properties
Transferrin	Trace amount	Transport of ferric iron If transferrin saturation > 45%, non–transferrin-bound iron forms If transferrin saturation > 75%, non–transferrin-bound iron/labile plasma iron forms, creating reactive radicals responsible for tissue damage
Ferritin	1–2 g in healthy subjects	Iron reservoir 4500 atoms Water soluble
Hemosiderin	0–1 g in healthy subjects	Similar to iron core of ferritin Results from ferritin degradation Not water soluble Forms clusters

Serum ferritin and transferrin levels are widely used to detect body iron overload. However, the level of serum ferritin may be affected by infections and inflammation states. Further, transferrin saturation may decrease in chronic iron deficiency, inflammation states, extensive malignancy, uremia, and nephrotic syndrome. Hence, because of these biologic confounders, blood markers should be used with caution to interpret the severity of iron overload (15).

Ultrasonography (US) does not allow detection or quantification of liver iron overload. Conventional single-energy computed tomography (CT) allows detection of iron overload by demonstrating increased attenuation of the liver parenchyma but is not sensitive or specific enough for grading or quantification of iron overload (16).

The liver is the organ of choice for biopsy, since liver iron content is strongly correlated with total body iron (1). Histologic grading of liver iron content is based on visual assessment of iron granules with Prussian blue stain at different magnifications. It is scored on a scale from 0 to 4, with 0 indicating absence of iron granules at ×400 magnification and 4 indicating iron visible at ×10 magnification or with the naked eye (17,18). This method is limited by its low intra- and interobserver repeatability (19,20).

Quantification of liver iron concentration with biochemical techniques, either with colorimetric or atomic absorption on deparaffinized tissue, constitutes the current reference method for histologic grading (18). Biochemical methods for quantification of liver iron content have been used in most magnetic resonance (MR) imaging

Table 2: Classification of Iron Overload Disorders

Classification	Causes	Key Clinical Manifestations
Hereditary hemochromatosis	Defect in *HFE* gene (most common) Mutations in ferroportin protein, transferrin receptor 2, hepcidin antimicrobial peptide *(HAMP)*, etc	Liver cirrhosis Heart failure Diabetes and bronze skin are late manifestations and are now rare owing to earlier diagnosis
Transfusional hemosiderosis		
β-Thalassemia major	Autosomal recessive disease Both β chains are abnormal, no hemoglobin A	Splenomegaly Bone deformities
Sickle cell disease	Autosomal recessive disease Mutations in both β chains; hemoglobin S, hemoglobin C, hemoglobin E	Vaso-occlusive crisis Acute chest syndrome Autosplenectomy
Myelodysplastic syndromes	Toxic effects on bone marrow due to toxicity of cancer treatment, radiation, or benzene	Most common in patient >60 years of age Acquired pancytopenia Increased risk of developing leukemia Increased risk of bleeding (low platelet count) Increased risk of infections (low white blood cell count)
Aplastic anemia	Pure red cell aplasia Blackfan-Diamond anemia Rare autosomal dominant genetic disease Multiple causes (autoimmune, secondary, idiopathic)	Blackfan-Diamond anemia Heterogeneous presentation of birth defects Higher risk of developing neoplasia including myelodysplastic syndromes, leukemia, and sarcomas

validation studies (21). Advantages of liver biopsy include the ability to evaluate multiple histopathologic changes, such as the presence and grade of liver iron, fat, inflammation, biliary disease, and fibrosis (2).

However, liver biopsy has limitations, some of which are inherent to the procedure and some of which are specific to assessment of liver iron. This technique is vulnerable to sampling error because it evaluates only a small tissue specimen (19,20). Studies have shown that there can be great intraorgan variability in liver iron content, especially in diseased liver; therefore, the specimen may not be representative if the iron deposition is heterogeneous (22,23). Wood et al (24) reported that liver MR imaging is more precise than liver biopsy for assessment of total body iron because of the former's lower sampling variability.

Liver biopsy has low acceptance by patients and physicians owing to concerns about pain, potential complications, high cost, low reimbursement, and logistic issues (25,26). This reluctance to undergo liver biopsy is further compounded by patients' increased awareness of the existence of alternative noninvasive techniques. While risk of severe intraperitoneal bleeding is generally perceived to be low—one in 2500 to one in 10 000 biopsies (20)—bleeding risk may be a concern and may even be strictly contraindicated in these patients, as the risk of bleeding is exacerbated by low platelet counts caused by liver insufficiency or hematologic disorders (27–29). There are other concerns about potential complications of infection, pneumothorax, hemothorax, and bowel perforation, especially if real-time image guidance is not used.

Over the past decade, technological developments have enabled MR imaging–based noninvasive techniques for quantitative assessment of liver iron overload. Many of these techniques, initially developed for research, have been adopted for clinical care and are now commercially available on clinical MR imaging units. Noninvasive quantification of iron with MR imaging is now considered the standard of care in diagnosis and monitoring of iron overload diseases (15). Some sequences are further refined for assessment of severe iron overload.

In this article, we describe the clinical applications of MR imaging–based liver iron quantification, including assessment of distribution, detection, grading, and monitoring of treatment response in iron overload. We review MR imaging–based quantification techniques. For each, we discuss the physical concepts, acquisition techniques, postprocessing, advantages, and limitations. We summarize the thresholds for different levels of iron overload severity and associated complications as well as the clinical thresholds for initiating

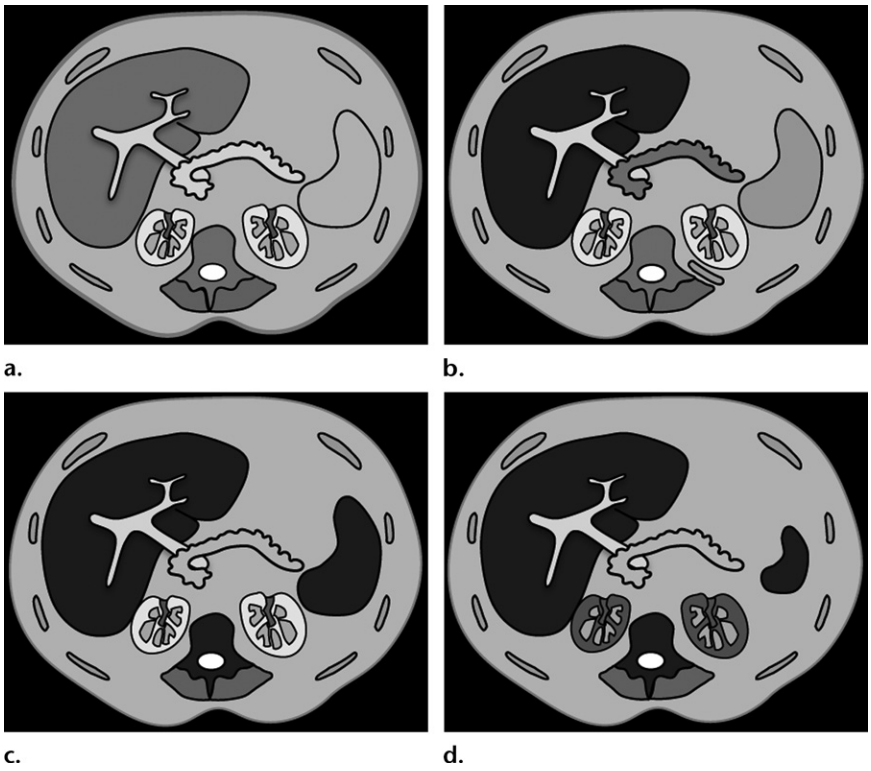

Figure 2. Relative signal intensity at MR imaging. **(a)** Normal signal intensity on T2- or T2*-weighted images. **(b)** In hemochromatosis, iron overload in the abdomen predominantly occurs in the liver and to a much lesser extent in the pancreas. **(c)** In transfusional hemosiderosis, iron overload in the abdomen occurs in the liver, spleen, and bone marrow, organs of the reticuloendothelial system. **(d)** In sickle cell disease, a form of hemolytic anemia, iron overload follows the same distribution as in transfusional hemosiderosis, but in addition the spleen may be small owing to autosplenectomy and the renal cortex may demonstrate iron overload owing to hemolysis of red blood cells and accumulation of iron in the proximal convoluted tubules. However, in practice, many variants are observed.

or adjusting therapy. We also provide an overview of the potential pitfalls and future directions.

Clinical Indications for Liver Iron Quantification

Distribution of Iron Overload

In hereditary hemochromatosis, iron overload in the abdomen initially occurs in the liver and pancreas. Non–transferrin-bound iron has a high affinity for hepatocytes (1,5).

In transfusional hemosiderosis, iron overload occurs in the reticuloendothelial system. This typically occurs by uptake of free iron by macrophages in the spleen and bone marrow and Kupffer cells in the liver (1).

In hemolytic anemia such as sickle cell disease, iron overload follows the same distribution as in transfusional hemosiderosis. However, the spleen may be small owing to autosplenectomy, and the renal cortex may also demonstrate iron overload owing to intravascular hemolysis of red blood cells and accumulation of unbound hemoglobin in the proximal convoluted tubules through filtration in renal glomeruli (27,30–32). Cortical kidney iron overload resulting from chronic hemolysis is common in sickle cell disease but not in thalassemia (33). Interestingly, kidney iron overload decreases in patients with sickle cell disease undergoing long-term transfusion who are receiving chelation therapy (33). However, in practice many variants are observed, as patients undergoing severe long-term transfusion often develop pituitary and pancreatic iron overload (34,35).

We illustrate the theoretical distribution of iron overload in abdominal organs for hemochromatosis, transfusional hemosiderosis, and sickle cell disease (Fig 2). Although iron overload can be seen in many organs, the liver is the main iron storage organ, the first to show iron overload, and the only one to show a linear relationship between its iron concentration and total body iron (36,37). Therefore, MR imaging for quantification of liver iron provides a good estimate of the degree of iron overload and allows prediction of the risk of complications.

Detection of Iron Overload

Clinical indications for iron detection with MR imaging include abnormally elevated ferritin or iron saturation, a high number of red blood cell transfusions, or a family history of hemochromatosis after genetic testing has been done, namely the search for C282Y and H63D mutations in the *HFE* gene. However, these genetic analyses do not cover all cases of hemochromatosis, and if the clinical history raises a suspicion of hereditary hemochromatosis, MR imaging should be performed to assess the severity and distribution of iron overload (7).

Detection of iron overload is important owing to the risk of complications such as myocardial disease, liver cirrhosis, and increased risk of hepatocellular carcinoma development in untreated

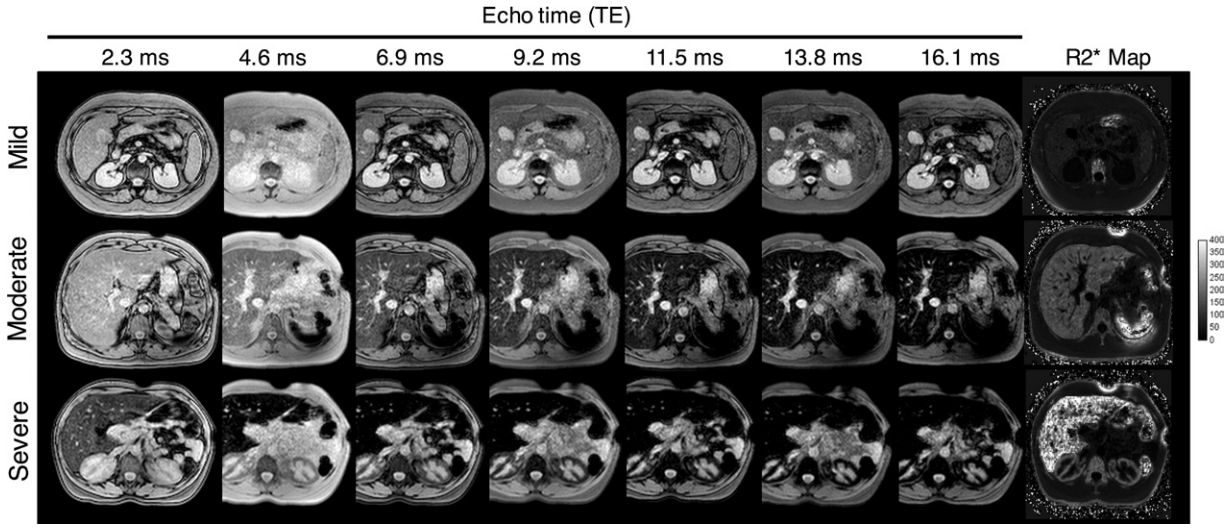

Figure 3. Transfusional hemosiderosis in three patients. Axial gradient-echo (GRE) MR images at 1.5 T with multiple echo times (TEs) (2.3, 4.6, 6.9, 9.2, 11.5, 13.8, and 16.1 msec) and corresponding R2* maps are shown. Top: Borderline mild iron overload in a 28-year-old woman with Blackfan-Diamond anemia. Low liver signal intensity is best seen with the longest TE (16.1 msec). R2* = 60 sec^{-1}. There is pancreatic fat infiltration with signal drop on the out-of-phase images (2.3, 6.9, 11.5, and 16.1 msec). Middle: Moderate iron overload in a 27-year-old man with sickle cell disease. Low liver signal intensity is best seen with an intermediate TE (6.9 msec). R2* = 140 sec^{-1}. There is marked iron overload in the spleen, which causes significant blooming on the longer TE images, limiting evaluation of the pancreatic tail and upper pole of the left kidney. Bottom: Severe iron overload in a 38-year-old woman with sickle cell disease. Low liver signal intensity is best seen with the shortest TE (2.3 msec). R2* = 310 sec^{-1}. There is renal cortical iron overload, suggesting recent intravascular hemolysis.

patients. Hence, it is critical to detect liver iron overload at an early stage and initiate treatment (discussed later) before the advent of complications (1).

Grading of Iron Overload

Grading the severity of iron overload in hemochromatosis and transfusional hemosiderosis (Fig 3) is helpful to guide initiation of proper treatment and help prevent future complications of untreated iron overload. Grading the degree of iron overload (as mild, moderate, or severe) can be performed subjectively or quantitatively (18). Subjective assessment of liver iron overload can be performed by comparing the signal intensity of the liver to that of other reference structures less prone to iron overload (such as paraspinal muscles) (38,39). Alternately, quantitative assessment is performed by measuring the degree of iron overload using one of the MR imaging–based quantification techniques discussed later. The measurement can then be converted to degree of iron overload on the basis of clinical thresholds.

Monitoring Treatment Response

Monitoring response to treatment in iron overload is required to adjust the most appropriate treatment with the least adverse effects. In hemochromatosis, the decision to initiate phlebotomy or adjust its frequency is typically based on the serum ferritin level. However, use of the serum ferritin level has some limitations: the initial serum ferritin level at the time of diagnosis does not accurately predict the number of phlebotomies required to reach normal liver iron concentration levels (40), and the subsequent serum ferritin levels do not decrease linearly with phlebotomy (41). While liver biopsy may in theory be used to monitor iron content mobilized by phlebotomies, it is usually reserved for staging of liver fibrosis in patients with hemochromatosis (42). Hence, MR imaging–based liver iron quantification has been proposed as a noninvasive alternative to liver biopsy both to predict the presence of fibrosis (43) and to monitor the progress of phlebotomy in hemochromatosis (29).

In transfusional hemosiderosis, the decision to initiate chelation therapy is based on a combination of serum ferritin level and liver iron content, which may be estimated with MR imaging–based techniques (44). The literature shows that serum ferritin level is an unreliable predictor of total body iron stores in thalassemia and sickle cell anemia (45,46). In patients with transfusional hemosiderosis, MR imaging relaxometry is superior to liver biopsy for monitoring liver iron content (24).

In thalassemia, transfusion is not the only physiologic event leading to iron overload. Ineffective erythropoiesis is an important factor leading to increased iron absorption. This physiologic event alone can lead to iron overload; thus, the numeration of blood transfusions alone cannot be used to identify the population at risk for iron overload.

Iron deposition in different organs can vary between patients, and MR imaging remains the only modality to allow evaluation of the distribution of nonhepatic iron stores (44). Moreover, sickle cell disease is known to cause an inflammatory state in which ferritin level is increased. Furthermore, organ iron deposition is directed only at patients who have received at least eight units of packed red blood cells.

The type of chelation and dose do not allow prediction of the efficacy of a treatment with enough certitude, and monitoring of organ deposition remains necessary considering the large variability in efficacy between individuals. Further, partial or absent response to treatment may indicate poor compliance with oral chelation therapy, which may require the addition of intravenous chelation therapy. Diseases leading to iron overload often cannot be treated curatively. Therefore, these patients are typically followed for years, and repeated liver biopsy is not an acceptable option for assessment of treatment response because of the reasons discussed earlier.

Qualitative and Quantitative Methods for Liver Iron Evaluation

Blood Tests

Iron overload is often initially detected on the basis of an abnormal serum transferrin level. Serum ferritin level generally increases with total body iron load, but this finding is not specific (47); ferritin level may be elevated in alcohol abuse, metabolic syndrome, or sideroblastic anemia, to name only a few conditions (48,49). Ferritin is an acute-phase protein, and as such its level can vary widely owing to inflammation, infection, liver damage caused by steatohepatitis or liver fibrosis, vitamin C levels, and even chelation therapy (47,50).

Therefore, serum ferritin is not an appropriate marker for diagnosis and monitoring of liver iron overload (15). Serum ferritin levels above 1000 μg/L warrant further evaluation to identify the cause of the iron overload, especially in the setting of hemochromatosis gene mutation, because such high levels of ferritin correlate with increased risk of death. The correlation of blood markers with iron body content is not as good as that of measurement with liver biopsy or MR imaging–based quantification (15).

Ultrasonography

US cannot be used to evaluate liver iron overload, whether qualitatively or quantitatively (16). However, it can be used to detect complications from iron overload, such as liver fibrosis, cirrhosis, portal hypertension, or hepatocellular carcinoma.

Computed Tomography

Conventional (single-energy) CT may allow detection of liver iron overload by showing increased attenuation but is not sensitive or specific. At nonenhanced CT, the attenuation of normal hepatic parenchyma usually ranges between 55 and 65 HU. Beyond that threshold, hepatic iron overload may be suspected (51). However, this threshold is not specific to iron overload, as other pathologic conditions can manifest with increased liver attenuation, such as Wilson disease, glycogen-storage diseases, or long-term amiodarone administration (51,52). Additionally, CT is associated with radiation and thus less appropriate for long-term monitoring, especially in young patients requiring repeated imaging throughout their lives (2).

Dual-energy CT is an emerging technique for iron quantification that requires comparison of liver attenuation on images obtained at two different kilovolt peak (kVp) settings with those of standardized cylinders of known iron concentration. With this method, reducing the kilovolt peak and kilo–electron volt (keV) values will show an increase in liver attenuation in the presence of iron overload and a decrease in the presence of steatosis. Further validations are still necessary before clinical application (53,54).

Biomagnetic Susceptometry

Biomagnetic liver susceptometry using a superconducting quantum interference device (SQUID) is an extremely sensitive technique that permits measurement of very small magnetic field variations, such as those induced by the presence of superparamagnetic liver iron. The correlation between liver iron content measured with biomagnetic susceptometry and that measured with liver biopsy has been proved to be excellent, and this technique is often considered the noninvasive reference standard for liver iron quantification (55). However, only a limited number of these devices are available worldwide, making this approach unavailable to most patients.

MR Imaging–based Iron Quantification Techniques

In this section, we review basic physics concepts relevant to MR imaging–based iron quantification. For each technique, we discuss the protocol, technical implementation, advantages, and limitations.

MR Imaging Physical Concepts

The presence of liver iron has multiple effects on the MR imaging signal, and several contrast mechanisms can be exploited to gain sensitivity to the presence of iron. For instance, liver iron, typically present in the form of ferritin or hemosiderin, will have an influence on the relaxation times

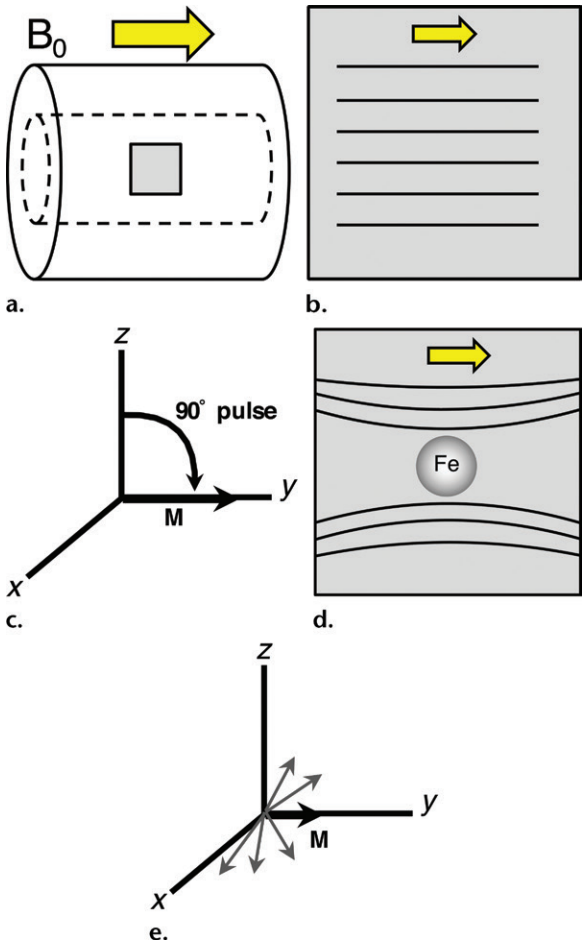

Figure 4. **(a)** The main magnetic field (B_0) is created by the MR imaging magnet. **(b)** A homogeneous main magnetic field provides a better-quality image. **(c)** After excitation, the magnetization *(M)* is in-phase. **(d)** The superparamagnetic effect of iron *(Fe)* (ferritin and hemosiderin) creates a local susceptibility-induced distortion in the local magnetic field. **(e)** This distortion causes magnetization dephasing, thus faster decay of the traverse magnetization, smaller net magnetization, and shorter T2 and T2*.

of the liver parenchyma, most notably T2 and T2*, and will also lead to a local alteration of the magnetic field, which can also be detected using phase-based methods such as quantitative susceptibility mapping.

T2 represents the time constant of the intrinsic decay of the transverse magnetization from spin-spin interactions, while T2* also incorporates effects from local magnetic field inhomogeneities: 1/T2* = 1/T2 + 1/T2', where T2' is the additional contribution from field inhomogeneities (56). T2 and T2* can also be represented as relaxivity rates, such that R2 = 1/T2, R2* = 1/T2*, and R2* = R2 + R2'. For example, a T2* of 5 msec would correspond to an R2* of 200 sec^{-1} (ie, R2* = 1/0.005 sec). The presence of liver iron will also lead to shortening of the longitudinal relaxation time constant T1, although this effect is generally weaker and not typically used for diagnosis of iron overload.

The superparamagnetic effect of ferritin and hemosiderin creates a local susceptibility-induced contribution to the local magnetic field that results in faster decay of the traverse magnetization (Fig 4), although the exact physical mechanisms involved differ for T2 and T2* relaxation (1). In both cases, the signal intensity on T2- and T2*-weighted images decreases with an increase in the iron concentration, as a result of shorter T2 and T2* constants (Fig 5) and an increase in R2 and R2*.

In clinical practice, gradient-echo (GRE) sequences are often used for their increased sensitivity to magnetic susceptibility (Table 3). As opposed to the presence of microscopic fat, which demonstrates a decrease in signal intensity on out-of-phase GRE images compared with in-phase images, the presence of liver iron overload will show decreased signal intensity on in-phase images compared with out-of-phase images. This phenomenon is due to the fact that in-phase images are typically acquired using a longer echo time (TE) than out-of-phase images, which leads to further decay of the signal secondary to the reduction in T2*.

Comparison of MR Imaging–based Iron Quantification Techniques

For each of the iron quantification techniques, we discuss acquisition techniques, acquisition protocols, postprocessing, advantages, and limitations. A summary of the key acquisition parameters of the MR imaging protocols is provided (Table 4) (21,38,57–59), as well as a summary of the advantages and limitations of each technique (Table 5) (2,59,60).

Liver-to-Muscle Signal Intensity Ratio

Concept.—The GRE-based signal intensity ratio technique is based on observation of a signal intensity decrease from T2* shortening in the presence of liver iron overload in comparison with the signal intensity of a reference tissue (assumed to be unaffected by iron content), typically the paraspinal muscles. The signal intensity of normal liver parenchyma (ie, without iron overload) should always be higher than that of the paraspinal muscles. Therefore, a hypointense liver relative to the paraspinal muscles indicates iron overload. This is assessed semiquantitatively by measuring the liver-to-muscle signal intensity ratio (2,38).

In severe iron overload, the signal intensity of the liver is lower than that of the paraspinal muscles even with sequences with limited sensitivity to iron overload (ie, T1-weighted and proton-density–weighted sequences). In moderate iron overload, lower signal intensity of the liver relative to that of the paraspinal muscles

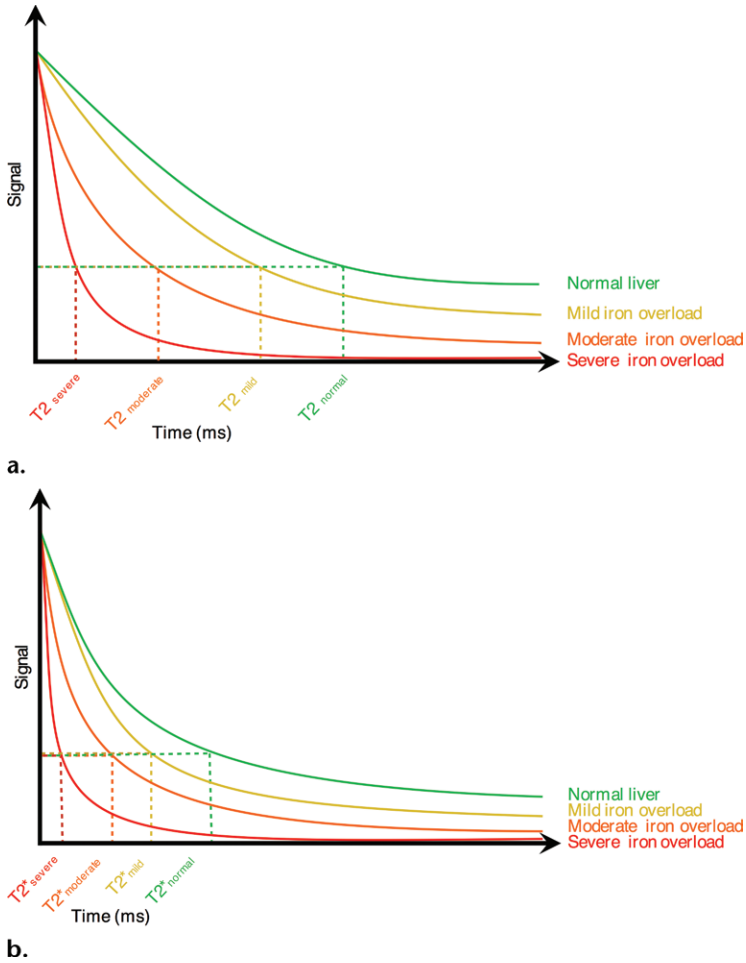

Figure 5. **(a)** T2 is the transverse relaxation and represents the decay rate constant from intrinsic spin-spin relaxation effects. R2 = 1/T2. Compared with normal liver (green), mild (yellow), moderate (orange), and severe (red) iron overload are associated with increasingly shorter T2 values (ie, increasingly higher R2 values). **(b)** T2* is similar to T2 but also includes the spin dephasing induced by the main magnetic field inhomogeneities. R2* = 1/T2*: for example, a T2* of 5 msec would correspond to an R2* of 200 sec^{-1} (ie, R2* = 1/0.005 sec). Compared with normal liver (green), mild (yellow), moderate (orange), and severe (red) iron overload are associated with increasingly shorter T2* values (ie, increasingly higher R2* values).

Table 3: Sequences for Iron Detection and Quantification

Sequences	Parameter Assessed	Findings
Iron detection		
Fast spin-echo T2-weighted	T2 shortening	Low liver SI relative to that of spleen
GRE T1-weighted dual-echo (in phase and out of phase)	T2* shortening	Signal drop on images with longer TE
Iron quantification		
Spin-echo multiecho	T2 shortening	Increasingly lower liver SI relative to that of spleen with longer TE
GRE PD-weighted multiecho	T2* shortening	Increasingly lower liver SI relative to that of spleen with longer TE
	Susceptibility	Increasingly higher magnetic susceptibility
GRE	Liver-to-muscle SI ratio in five sequences with T1, PD, T2, T2+, and T2++ weighting	Low liver SI relative to that of paraspinal muscles

Note.—PD = proton density, SI = signal intensity.

is seen with sequences that are moderately sensitive to iron overload (ie, T2*-weighted sequences with intermediate TE). In mild iron overload, lower signal intensity of the liver relative to that of the paraspinal muscles is seen with sequences that are most sensitive to iron overload (ie, heavily T2*-weighted sequences with long TE) (38).

Protocol.—At 1.5 T, five GRE sequences are performed during separate breath holds with a constant repetition time of 120 msec, a constant flip

Table 4: Sequence Acquisition Parameters for Iron Detection and Quantification

Parameters	Signal Intensity Ratio	T2 and R2 Relaxometry	T2* and R2* Relaxometry	Quantitative Susceptibility Mapping
Sequences	GRE	Multisection single spin-echo	Multiple single-echo GRE or single multiecho GRE	Multiecho GRE
Breathing	Breath holding	Free breathing	Breath holding	Breath holding
Typical TR (msec)	120	2500	25	14
TEs for 1.5-T imaging (msec)	2 (T1W) 4 (PDW) 9 (T2*W) 14 (T2*+W) 19 (T2*++W)	6, 9, 12, 15, 18	The original Wood protocol included multiple breath holds, each with echoes ranging from 0.8 msec to 4.8 msec at 0.25-msec intervals More recent approaches use a single breath-hold, single TR, multiecho sequence	Multiple echoes (may vary)
Flip angle (degrees)	20	90	20	5

Note.—PDW = proton-density–weighted, T1W = T1-weighted, TR = repetition time, T2*W = T2*-weighted, T2*+W = T2*+-weighted, T2*++W = T2*++-weighted.

Table 5: Comparison of Techniques for Liver Iron Quantification

Techniques	Advantages	Limitations
Signal intensity ratio	Simplest method Widely available Free web-based calculator for 1.0-T, 1.5-T, and 3.0-T imaging	Not accurate for severe iron overload (>350 μmol/g dry tissue [>19.5 mg/g]) Assumes that reference tissue (paraspinal muscles) is normal
T2 and R2 relaxometry	Validated method with FerriScan (Resonance Health; Burswood, Western Australia, Australia)	Long acquisition time Prone to respiratory motion artifacts Available only for 1.5-T imaging Technically difficult to implement Additional cost and delay for analysis
T2* and R2* relaxometry	Fast acquisition time Single or multiple breath holds (depending on protocols) Allows detection of a wide range of liver iron content Postprocessing algorithms now available for recent MR imaging systems Available for 1.5-T and 3.0-T imaging	Postprocessing algorithms are not universally available and must be purchased
Quantitative susceptibility mapping	Highest sensitivity for detecting iron deposition All acquisitions in a single breath hold Algorithms correcting for presence of fat Susceptibility values can be compared regardless of field strength	Still used only in research Correlation between quantitative susceptibility mapping values and liver iron content not yet clearly established

angle of 20°, and varying TE to achieve different weighting: a T1-weighted sequence with TE of 2 msec, a proton-density–weighted sequence with TE of 4 msec, and T2*-weighted sequences with increasingly long TEs of 9 msec, 14 msec, and 19 msec. This protocol was updated in September 2017, with small modifications made to the first and last sequences since an earlier version (38).

For this protocol, a body coil should be used to ensure homogeneous transmission and reception of the signal to optimize image quality and minimize artifacts, since surface coils tend to produce higher signal intensity close to the coil (38). With the signal intensity ratio technique, out-of-phase TEs are intentionally avoided because this would cause ambiguity in the interpretation of

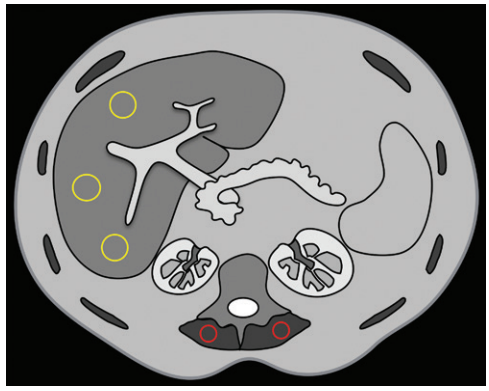

Figure 6. The liver-to-muscle signal intensity ratio technique requires measurement of the signal intensity with three ROIs in the liver (yellow circles), excluding vascular structures, and one ROI in each paraspinal muscle (red circles) with five MR imaging sequences, in which repetition time and flip angle are held constant while varying TE to alter the T1 and T2* weighting. These values are used to compute five different liver-to-muscle signal intensity ratios, which are then analyzed with the algorithm developed by Gandon et al (38) and provided on the website of the University of Rennes.

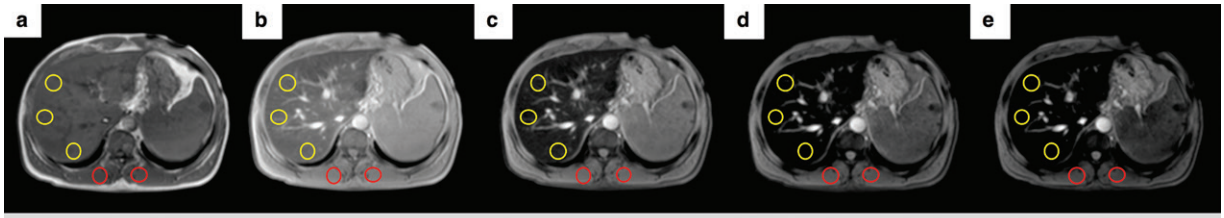

	a	b	c	d	e
TR (msec)	120	120	120	120	120
TE (msec)	4.6	4.6	9.2	13.8	18.3
FA (°)	90	20	20	20	20

Figure 7. Moderate liver iron overload due to hemosiderosis in a 57-year-old man with β-thalassamia hemoglobin C. Multiecho axial MR images at 1.5 T were obtained according to an earlier Rennes protocol, with TEs of 4.6 msec (T1-weighted) *(a)*, 4.6 msec (proton-density–weighted) *(b)*, 9.2 msec (T2-weighted) *(c)*, 13.8 msec (T2+-weighted) *(d)*, and 18.3 msec (T2++-weighted) *(e)*. Three ROIs were drawn in the liver (yellow circles) and one in each paraspinal muscle (red circles) for each of the five sequences. Associated splenomegaly is seen. Liver iron content was 160 μmol/g ± 50 (8.9 mg/g dry weight ± 2.8) according to the Rennes protocol.

signal drop, which could not be unequivocally attributed to iron or fat overload. The acquisition time is 15 seconds per sequence, and total examination time is about 2 minutes (2).

Acquisition protocols are provided online for MR imaging field strengths of 1.0 T, 1.5 T, and 3.0 T (38,61). The author who originally developed this technique recently demonstrated the feasibility of the signal intensity ratio approach at 3.0 T (39).

Measurement Method.—This technique requires measurement of the signal intensity in five regions of interest (ROIs) of about 1 cm^2. Three of them are drawn in the liver parenchyma, excluding vascular structures, and one is drawn in each paraspinal muscle (Fig 6). The process is repeated with the five MR imaging sequences described earlier (Fig 7) (61).

Postprocessing.—The values obtained with measurement of the ROIs are used to compute five different liver-to-muscle signal intensity ratios, which are then analyzed with the algorithm developed by Gandon et al (38) and implemented on a free web-based calculator hosted by the University of Rennes (Fig 8) (61).

Advantages.—This is the simplest method for quantification of liver iron overload, requiring the least amount of postprocessing. The technique can be implemented on a wide array of MR imaging units from different vendors. The acquisition parameters required and the postprocessing calculations are provided free by the developers of the technique. Furthermore, this technique at 3.0 T will be more sensitive to milder liver iron overload (2,38,39).

Limitations.—This technique is not accurate for severe iron overload exceeding 350 μmol/g dry weight (19.5 mg/g dry weight) and tends to overestimate mild and moderate liver iron overload. This is why use of the signal intensity ratio method—although still available online—is discouraged by the developer of the technique, who now recommends use of a multiecho GRE protocol and provides a free Java application that permits off-line calculation of liver iron content on the basis of the signal intensity ratio and T2* (38,61). Further, the technique is dependent on the assumption that the reference tissue is normal. While paraspinal muscles should not be affected by iron overload, muscle atrophy and fat infiltration, especially in elderly patients, may confound the T1 and T2* of the muscles (38,39). Spatial inhomogeneity of signal from B_0 or B_1 inhomogeneity effects at 3.0 T may represent an additional limitation.

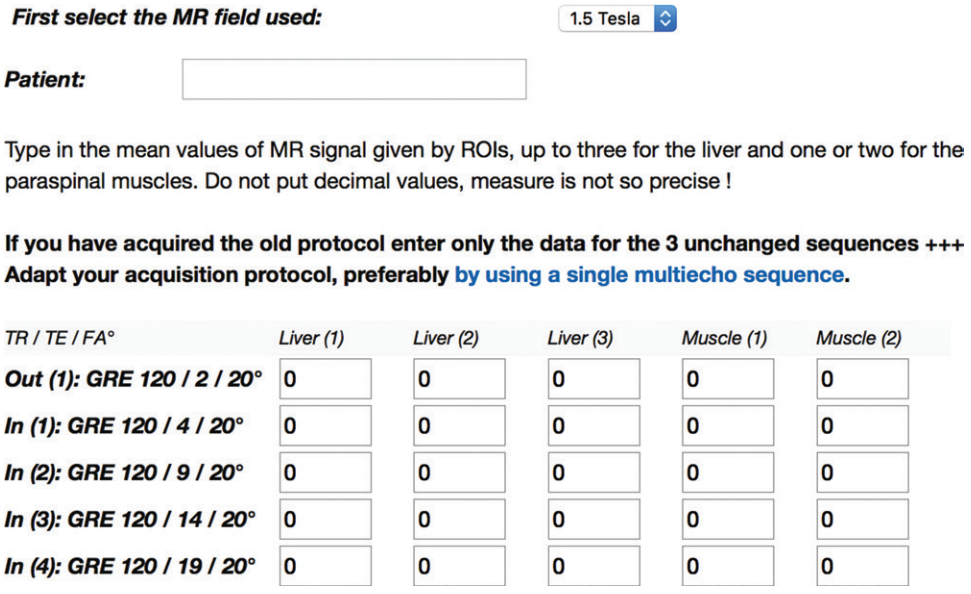

Figure 8. Screen shot from the website of the Rennes protocol algorithm. The ROI values are inserted in the table, and the estimated liver iron concentration is computed online. The algorithm is currently available for 1.0-T, 1.5-T, and 3.0-T field strengths. *FA* = flip angle, *TR* = repetition time.

T2 and R2 Relaxometry

Concept.—Although the precise mechanism by which T2 and R2 relaxometry is affected by the presence of iron has not been clearly established, two mechanisms have been proposed to explain T2 shortening in the presence of iron overload. The first theory suggests that proton exchange between bulk water and exchangeable protons on the surface of the ferritin core affects the relaxation rate of the protons locally (62). The second theory explains that hemosiderin clusters induce a magnetic field inhomogeneity, which causes a relaxation mechanism based on diffusion of protons (63). These two mechanisms may contribute to decrease of T2 and increase of R2 in the presence of iron. The technique known as R2 relaxometry has been validated by St Pierre et al (21) and is approved by the U.S. Food and Drug Administration (FDA). It is commercialized as FerriScan (Resonance Health) (64).

Protocol.—At 1.5 T, R2 relaxometry requires a multisection single spin-echo sequence during free breathing to obtain axial images with repetition time of 2500 msec, TE every 3 msec from 6 msec to 18 msec (at 6, 9, 12, 15, and 18 msec), flip angle of 90°, section thickness of 5 mm, matrix size of 256, and field of view between 350 and 400 mm, depending on the patient's habitus (21). A bag of saline solution or Ringer solution is placed in the field of view to serve as an internal control.

Measurement Method.—To develop the calibration curve that links the R2 measurement with the liver iron concentration, the developers of this technique selected an ROI covering the right liver lobe on the largest axial section of the liver. The details of the measurement technique are not provided for the commercial implementation of R2 relaxometry (21).

Postprocessing.—Postprocessing requires transfer of images acquired according to the recommended protocol of Resonance Health. A weighted biexponential model that includes corrections for signal gain drift, noise bias, and radiofrequency field inhomogeneities is fitted to the image signal intensities measured at each TE to calculate R2, then the liver iron content is estimated by using the calibration curve developed by St Pierre and colleagues (21,37,65). The image analysis is performed remotely, and results are returned with a color parametric map of R2 (37,64).

Advantages.—R2-measured liver iron content correlates well with biopsy liver iron content in a nonlinear fashion. Images are acquired during free breathing, which may be more comfortable for patients unable to hold their breath, such as young children and fragile patients. The company provides assistance for calibration of the MR imaging unit and quality control, thus making this approach more convenient for centers with a lower volume of examinations or less familiarity with the physical concepts (21,37,64).

Limitations.—Because of the nonlinear relation, liver iron content values measured with R2 relaxometry become more variable in higher iron overload when liver iron content is over 20 mg/g dry weight, making liver iron content calculation less precise. FerriScan is the only commercially available R2 relaxometry iron quantification technique. Coexisting liver steatosis is problematic, since fat saturation is not used. It requires a long acquisition

time, up to 20 minutes while freely breathing, making it prone to respiratory motion artifacts and thus not practical in the setting of restrained resources of equipment and time (37). The lack of fat saturation of the subcutaneous fat can also cause a ghosting effect in the liver with respiratory motion.

It also requires additional cost and delay for the data analysis, with the company's target time being within 2 business days (64). Therefore, post hoc addendums to radiology reports may be made after the company's report is available.

T2* and R2* Relaxometry

Concept.—As explained earlier, liver parenchymal iron overload causes T2* to decrease and R2* to increase owing to a combination of the T2 (R2) effects and the microscopic inhomogeneities introduced in the main magnetic field (B_0) by the superparamagnetic properties of hemosiderin clusters (58).

Protocol.—In the original description of the technique, GRE sequences with multiple breath holds were used to obtain axial images with repetition time of 25 msec, TEs every 0.25 msec from 0.8 msec to 4.8 msec, flip angle of 20°, section thickness of 15 mm, matrix size of 64 × 64 and field of view of 48 × 24 mm, depending on the patient's habitus, and bandwidth of 83 kHz (58). More recently, single breath-hold multiecho GRE sequences have been widely adopted, both in research and the clinical setting (22,66). Multiple variants of multiecho protocols have been described in the literature. However, there has not been consensus on the recommended acquisition parameters for assessment of R2* (30,67,68).

Measurement Method.—Wood et al (58) measured the R2* from a single midhepatic section by drawing an ROI following the boundaries of the liver and excluding hilar vessels to obtain an R2* map.

Postprocessing.—Wood et al (58) described the relationship between liver iron content and R2* with the following equation: [Fe] = 0.202 + 0.0254R2*. To use this equation to estimate the MR imaging–based liver iron content, acquisition protocols should be similar to the one described by Wood et al (58). There have been some other calibration curves for liver iron content and R2* proposed in the past few years, all fairly similar (30,67,68).

Advantages.—In multiple studies, R2* has been demonstrated to have a linear correlation with biopsy-determined liver iron content, which makes R2* relaxometry a reliable technique for noninvasive liver iron overload quantification (58). Multiecho GRE MR imaging techniques are more practical, as they are faster and permit simultaneous quantification of liver steatosis and iron overload in a single breath hold, thus reducing motion artifacts and optimizing acquisition time (22,66). Liver iron content can be estimated at 1.5 T and 3.0 T, and this technique enables detection of a wide dynamic range, from mild (Fig 9) to severe.

Limitations.—Use of 3.0-T imaging will reduce the upper measurable range limit of liver iron content by two owing to the faster decay of the signal. The R2* at 3.0 T has been shown to be twice that at 1.5 T (2,58). At 1.5 T, R2* relaxometry has been shown to be limited in very severe iron overload with liver iron content higher than 30 mg/g dry weight (37). The postprocessing algorithms are commercially available only as a purchaseable option and may not be universally available. A limitation of this technique is the other contributors to B_0 inhomogeneity, such as air and metal, and dependence on voxel geometry (69).

Quantitative Susceptibility Mapping

Concept.—The presence of a local susceptibility source such as ferritin or hemosiderin leads to an augmentation of the local magnetic field, which has an impact on the measured phase of a GRE sequence. Using an acquisition with two or more echoes, the local magnetic field can be estimated, and the inverse problem relating the measured magnetic field distribution to the underlying susceptibility distribution can be solved (70).

Protocol.—Abdominal quantitative susceptibility mapping can be performed using a three-dimensional breath-hold multiecho GRE sequence. With appropriate parameters, such an acquisition can be used to simultaneously perform chemical shift–encoded water/fat separation, T2*/R2* mapping, and B_0 field mapping, from which a quantitative susceptibility map can be reconstructed (59,71).

Measurement Method.—After calculation of the quantitative susceptibility map, a local relative susceptibility value (ΔB_0), generally expressed in parts per million (ppm), can be extracted from an ROI. That susceptibility value can be related to the liver iron content.

Postprocessing.—Calculation of a quantitative susceptibility map requires several postprocessing steps (Fig 10). The first step is generally to estimate a B_0 field map from the acquired data. In the case of abdominal applications, for which the presence of fat is expected, this is ideally

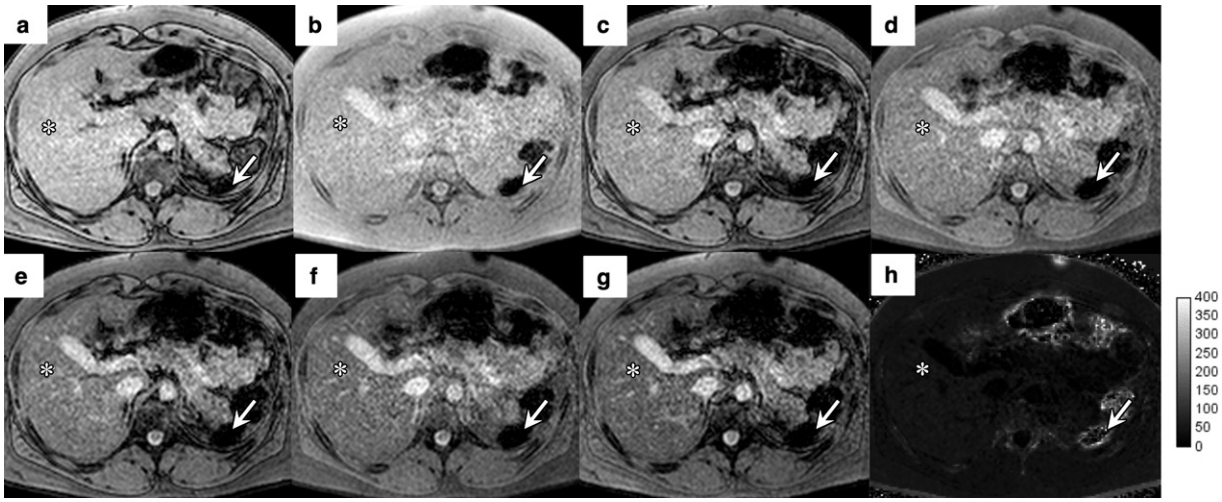

Figure 9. Mild liver iron overload due to hemosiderosis in a 29-year-old woman with sickle cell disease. *(a–g)* Multiecho axial MR images at 1.5 T with TEs of 2.3 msec *(a)*, 4.6 msec *(b)*, 6.9 msec *(c)*, 9.2 msec *(d)*, 11.5 msec *(e)*, 13.8 msec *(f)*, and 16.1 msec *(g)*. *(h)* Corresponding R2* map shows severe iron overload in a small spleen due to autosplenectomy (arrow) and normal R2* (45 sec^{-1}) in the liver (*). The liver iron concentration according to the Rennes protocol (not shown) was 40 μmol/g ± 20 (2.5 mg/g dry weight ± 1.1), which indicated borderline mild iron overload.

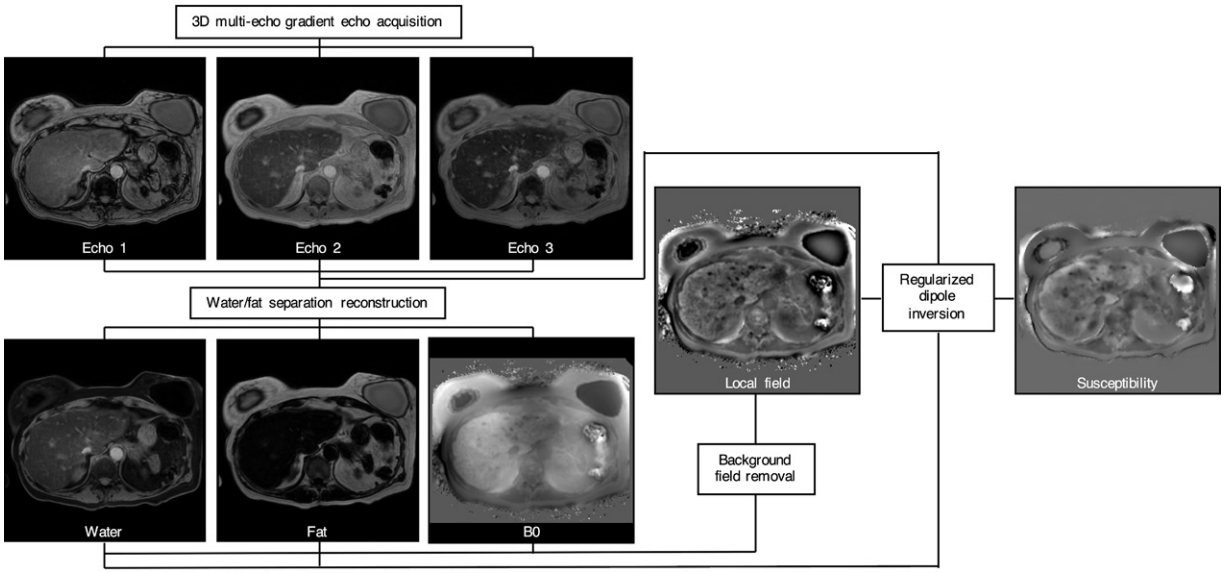

Figure 10. Flowchart of processing steps for quantitative susceptibility mapping. *3D* = three-dimensional.

performed using a chemical shift–encoded reconstruction, to separate the contribution of susceptibility sources from the contribution of chemical shift effects in the measured phase.

The magnetic field from local sources is then estimated from the overall magnetic field, and the underlying susceptibility distribution is reconstructed by solving the corresponding inverse problem. In practice, some of these steps can be combined. The inversion from magnetic field to susceptibility typically requires anatomic regularization, given the ill-posed nature of the problem (59,70,71).

Advantages.—Quantitative susceptibility mapping is potentially the most direct and most sensitive MR imaging technique for detection of iron deposition. Furthermore, all acquisitions are typically performed in a single breath hold, reducing to a minimum the risk of motion. Recent algorithms can correct for the presence of fat. Additionally, susceptibility values can be compared regardless of the field strength (Fig 11).

Limitations.—Quantitative susceptibility mapping is still used only in research, is not standardized, and is not offered commercially by the main MR imaging manufacturers. The exact relationship between quantitative susceptibility mapping values and liver iron content is not yet clearly established. Further research on its

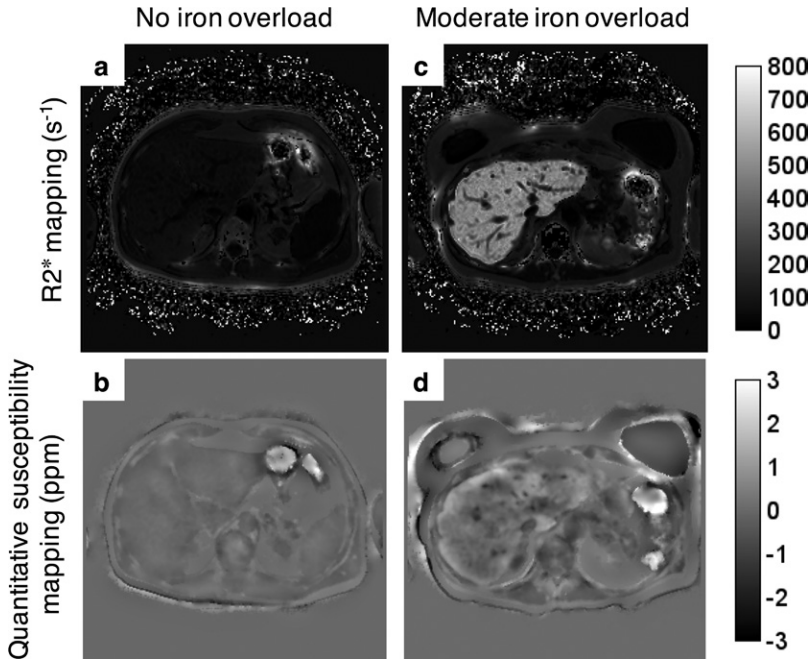

Figure 11. R2* map *(a)* and quantitative susceptibility map *(b)* in a subject without iron overload. R2* map *(c)* and quantitative susceptibility map *(d)* in a patient with moderate iron overload.

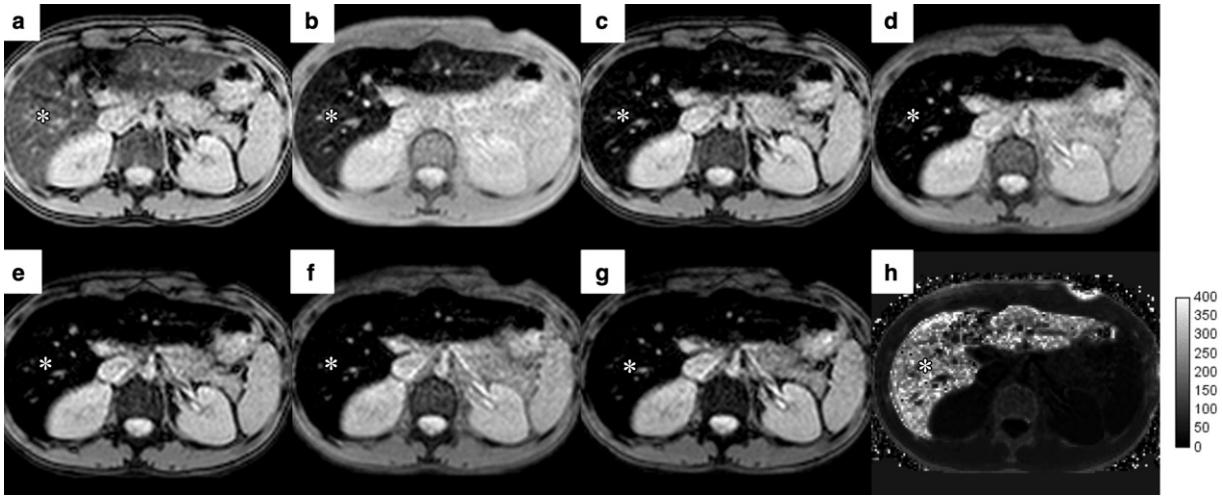

Figure 12. Liver iron overload in a 20-year-old woman with juvenile hemochromatosis (homozygous *HFE2* mutation) and without any history of alcohol abuse. *(a–g)* Multiecho axial MR images at 1.5 T with TEs of 2.3 msec *(a)*, 4.6 msec *(b)*, 6.9 msec *(c)*, 9.2 msec *(d)*, 11.5 msec *(e)*, 13.8 msec *(f)*, and 16.1 msec *(g)*. *(h)* Corresponding R2* map shows iron overload in the liver (*), with R2* = 230 sec^{-1}. The liver iron concentration according to the Rennes protocol (not shown) was 270 μmol/g ± 50 (15.0 mg/g dry weight ± 2.8), which indicated moderate-severe iron overload.

accuracy and reproducibility will be needed to establish it as a future valuable liver iron quantification technique (2,59).

Clinical Applications of MR Imaging–based Iron Quantification Techniques

MR imaging–based iron quantification techniques may be used to assess the distribution and severity of disease. In addition, these techniques are required to monitor liver iron overload for adjustment of phlebotomy (in hereditary hemochromatosis) and to evaluate response to or compliance with chelation therapy in hereditary hemochromatosis and transfusional hemosiderosis (mainly β-thalassemia and sickle cell disease).

Hemochromatosis is a genetic disease caused by genetic mutations in the *HFE* gene, leading to increased absorption of iron in the duodenum and iron overload, primarily in the liver, heart, pancreas, and pituitary gland (72,73) (Fig 12). Since physiologic iron excretion occurs by cellular exfoliation, menstruation, or other causes of bleeding, the ability to eliminate excess iron is limited (74). Hence, the main goal of treatment is to increase iron excretion. Since patients with hemochromatosis do not have blood dyscrasia, phlebotomies may be performed to reduce iron

Table 6: Use of Phlebotomy in Hemochromatosis

Parameter	Elevated Level	Threshold for Initiating Therapy	Threshold for Adjusting Therapy
Serum ferritin level (μg/L)	>200 (women) >300 (men)	<120	<110 for 3 weeks
Use of phlebotomy	500 mL weekly	Every 2 weeks	Discontinue

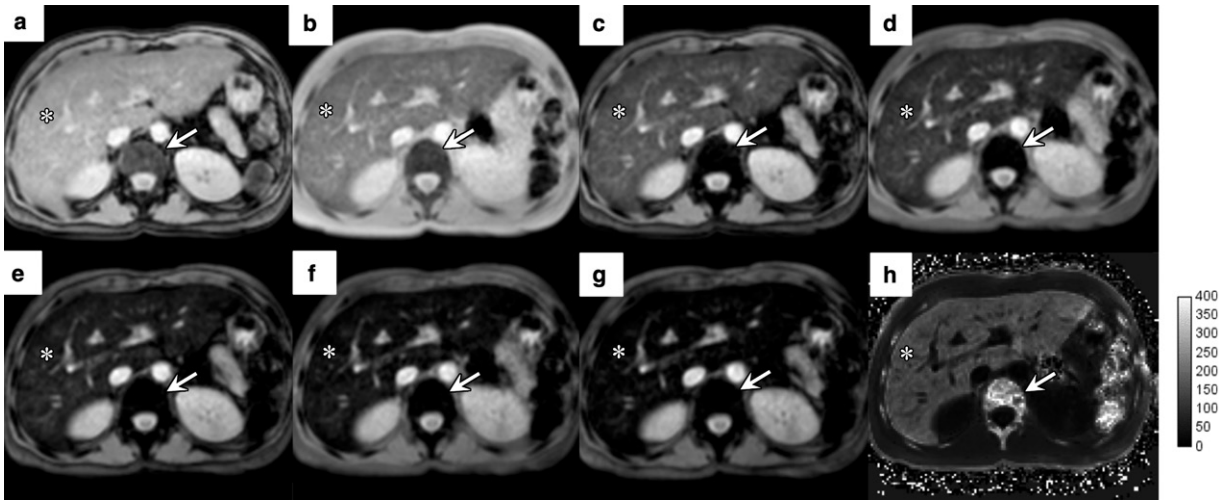

Figure 13. Mild-moderate liver iron overload due to hemosiderosis in a 33-year-old woman with β-thalassemia type hemoglobin E. The patient had undergone splenectomy. *(a–g)* Multiecho axial MR images at 1.5 T with TEs of 2.3 msec *(a)*, 4.6 msec *(b)*, 6.9 msec *(c)*, 9.2 msec *(d)*, 11.5 msec *(e)*, 13.8 msec *(f)*, and 16.1 msec *(g)*. *(h)* Corresponding R2* map shows severe iron overload in the bone marrow (arrow) and mild-moderate iron overload in the liver (*), with R2* = 135 sec^{-1}. The liver iron concentration according to the Rennes protocol (not shown) was 160 μmol/g ± 50 (8.9 mg/g dry weight ± 2.8), which indicated moderate iron overload.

overload and prevent complications. Initiation and adjustment of the frequency of the phlebotomies are currently based on the ferritin level, aiming for ferritin levels between 50 and 100 μg/L, according to the practice guideline of the American Association for the Study of Liver Diseases (AASLD) (Table 6) (15).

β-thalassemia major is a genetic disease caused by genetic mutations, leading to severe anemia requiring repeated transfusions; otherwise death usually occurs in late childhood. Cardiac complications are the leading cause of mortality among patients who are not treated efficiently (15,75). Early treatment and monitoring are thus critical to minimize those important potential complications. The primary treatment of β-thalassemia major consists of blood transfusion, which is needed repeatedly to improve anemia and suppress ineffective erythropoiesis. However, while long-term transfusion prevents complications of β-thalassemia, it also leads to accumulation of iron, which is mainly stored in the reticuloendothelial system (Fig 13).

Chelation therapy is therefore required in patients who develop iron overload to prevent toxic effects associated with large amounts of exogenous iron. These medications bind iron in the body to be excreted in the urine and/or stool. Deferoxamine, deferiprone, and deferasirox are the principal medications used.

Deferoxamine, the chelator that has been used for decades and is thus the best known, is administered subcutaneously or intravenously by the patient him- or herself at least 4 days a week for 8–12 hours, leading to compliance problems due to the high cost of the material needed, the cumbersome tubing and pump, and possible local complications such as infections and pain at the injection site. Toxic reactions to this medication may lead to retinal, auditory, and sensory neural damage.

Deferiprone, an oral chelator, is taken three times a day, and patients are generally more compliant than with intravenous treatment. The most common side effects are gastrointestinal (such as abdominal discomfort or pain, nausea, and emesis). Myalgia and joint pain are also reported, resolving with medication cessation. More serious complications include variable degrees of neutropenia, which could be as severe as agranulocytosis, which is usually reversible when medication

Table 7: Chelation Therapy in Transfusional Hemosiderosis

Parameter	Threshold for Initiating Therapy	Threshold Indicating Inadequate Chelation
Number of transfusions	After the first 10–20 transfusions (in β-thalassemia)	...
Cardiac T2* at 1.5 T (msec)	<20	<15
Liver iron content (mg/g dry weight)	>7	>15
Liver R2* at 1.5 T (sec^{-1})*	>270	>580
Serum ferritin level (μg/L)	>1000	>2500

*Extrapolated from the liver iron content according to a calibration curve from Wood et al (58).

is stopped but is still potentially deadly. For this reason, patients must be followed regularly with complete blood cell counts to identify cases of agranulocytosis.

Deferasirox, an oral chelator, is taken only once daily and may cause gastrointestinal side effects. Hepatic and renal failure have been reported; thus, this treatment is contraindicated in patients with prior liver or renal dysfunction.

Combinations of different chelators are often needed to achieve optimal control of iron overload. In North America, patients usually have to choose between deferiprone and deferasirox, the latter being most frequently chosen. Differential efficacy according to site of iron overload has been documented, with deferiprone preferentially suggested for iron overload of the heart, mainly in thalassemia patients (27). Monitoring and adjustment of chelation therapy are based on liver iron concentration as assessed with MR imaging. Monitoring of iron overload is recommended starting in early childhood and is necessary all life long, since β-thalassemia major is not a curable disease (27,29).

The same principles apply to sickle cell disease, which is a genetic disorder of the hemoglobin, leading to abnormal red blood cells causing hemolytic anemia. In addition to iron accumulation in the reticuloendothelial system, these patients may also demonstrate iron overload in the renal cortex owing to the hemolytic component of the disease. Other hereditary anemias, such as Blackfan-Diamond anemia, also necessitate long-term blood transfusions, leading to iron overload at a young age with subsequent risk of cardiac toxic effects (35).

Monitoring of chelation therapy is based on liver iron content as assessed with MR imaging instead of liver biopsy (Table 7). Annual liver iron quantification with MR imaging is recommended for patients undergoing long-term transfusion, starting at the age of initial diagnosis (15,35).

We provide a summary of the clinical thresholds for serum analysis and MR imaging–based quantification for different levels of iron overload severity (Table 8). We used a linear calibration equation (Wood et al [58]) to calculate the T2* and R2* from the threshold values of liver iron content used in treatment algorithms for iron overload pathologic conditions (72).

Future Directions

Ultrashort-TE Sequences

Inability to accurately quantify very severe iron overload owing to very short T2* is a limitation of commercially available MR imaging–based iron quantification techniques. This constraint is exacerbated at higher field strength owing to faster T2* decay (twice as fast at 3.0 T as at 1.5 T) (76). When iron overload is very severe, with levels over 25 mg/g dry weight at 1.5-T imaging, corresponding to T2* of 1 msec or less, the signal drops below the noise floor, leading to overestimation of T2*—and thus underestimation of iron overload—owing to inaccurate curve fit (Fig 14).

Ultrashort-TE sequences with TE as low as 0.1 msec are achievable and would permit quantification of massive iron overload, even at 3.0 T. In comparison, the shortest TE achievable with current GRE sequences is in the range of 0.8 msec. Preliminary results suggest that ultrashort-TE sequences may represent a viable replacement for or alternative to conventional GRE sequences for R2* estimation, for both low and high iron overload (76).

Multiparametric Assessment

Chronic liver diseases are characterized by the concomitant presence of pathologic changes, including liver fat, iron, inflammation, biliary disease, and fibrosis (77). Further, the coexistence of several pathologic changes may act as a confounder to liver iron quantification, affecting the R2 or R2* of tissue. Eventually, multiparametric techniques will be required to assess each of these pathologic parameters and control these biologic confounders.

Hence, a comprehensive multiparametric quantitative MR imaging protocol may include elastography sequences for assessment of liver

Table 8: Liver Iron Concentration Measured with Liver Biopsy, Biochemical Techniques, and MR Imaging and Risk of Complications

Measurement Techniques and Complication Risk	Normal Values	Degree of Iron Overload		
		Mild	Moderate	Severe
Liver biopsy				
Liver iron content (mg/g dry weight)	<1.8	3.2–7.0	7.0–15.0	>15.0
Biochemical techniques				
Serum ferritin (μg/L)	<200 premenopausal women <300 men	1000–2500	1000–2500	>2500
Transferrin saturation (%)	20–50	>50	>50	>50
Alanine aminotransferase (U/L)	<250	>250	>250	>250
MR imaging				
Iron concentration Rennes protocol at 1.5 T (μmol/g [mg/g])	<40	40–100 (2.2–5.6)	100–300 (5.6–16.7)	>300 (>16.7)
R2 at 1.5 T (sec^{-1})*	<45	60–100	100–160	>160
R2 at 3.0 T (sec^{-1})†	<90	130–200	200–320	>320
T2* at 1.5 T (msec)	>16	8–4	4–2	<2
R2* at 1.5 T (sec^{-1})‡	<60	120–270	270–580	>580
T2* at 3.0 T (msec)	>8	4–2	2–1	<1
R2* at 3.0 T (sec^{-1})	<126	240–540	540–1160	>1160
Increased risk of complications				
General complications	−	+	++	+++
Cardiac complications	−	−	−	++

Note.—Owing to ongoing standardization of liver iron quantification techniques, calibration curves, and grading thresholds, there may be discrepancies in the severity of liver iron overload as determined with visual assessment or different quantitative techniques.
*Extrapolated from the liver iron content according to a calibration curve from St Pierre et al (21).
†Extrapolated from the 1.5-T values.
‡Extrapolated from the liver iron content according to a calibration curve from Wood et al (58).

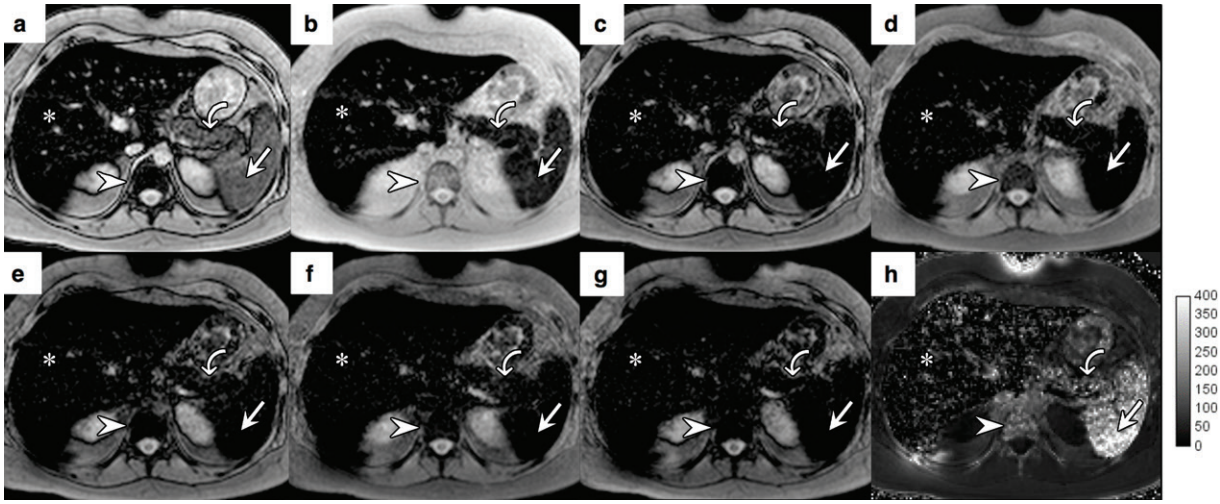

Figure 14. Very severe liver iron overload due to hemosiderosis in a 31-year-old woman with aplastic anemia and erythroblastopenia. *(a–g)* Multiecho axial MR images at 1.5 T with TEs of 2.3 msec *(a)*, 4.6 msec *(b)*, 6.9 msec *(c)*, 9.2 msec *(d)*, 11.5 msec *(e)*, 13.8 msec *(f)*, and 16.1 msec *(g)*. *(h)* Corresponding R2* map shows unreliable R2* values in the liver (*) and severe iron overload in the spleen (straight arrow), pancreas (curved arrow), and bone marrow (arrowhead). R2* quantification is unreliable because the signal is below the noise floor owing to very severe iron overload. There is no iron overload in the renal cortex. Also note the signal drop between in-phase acquisition *(b)* and out-of-phase acquisition *(a)*, indicating fat in the bone marrow, thus contributing to some degree to the low signal intensity seen in the bone marrow on the out-of-phase images.

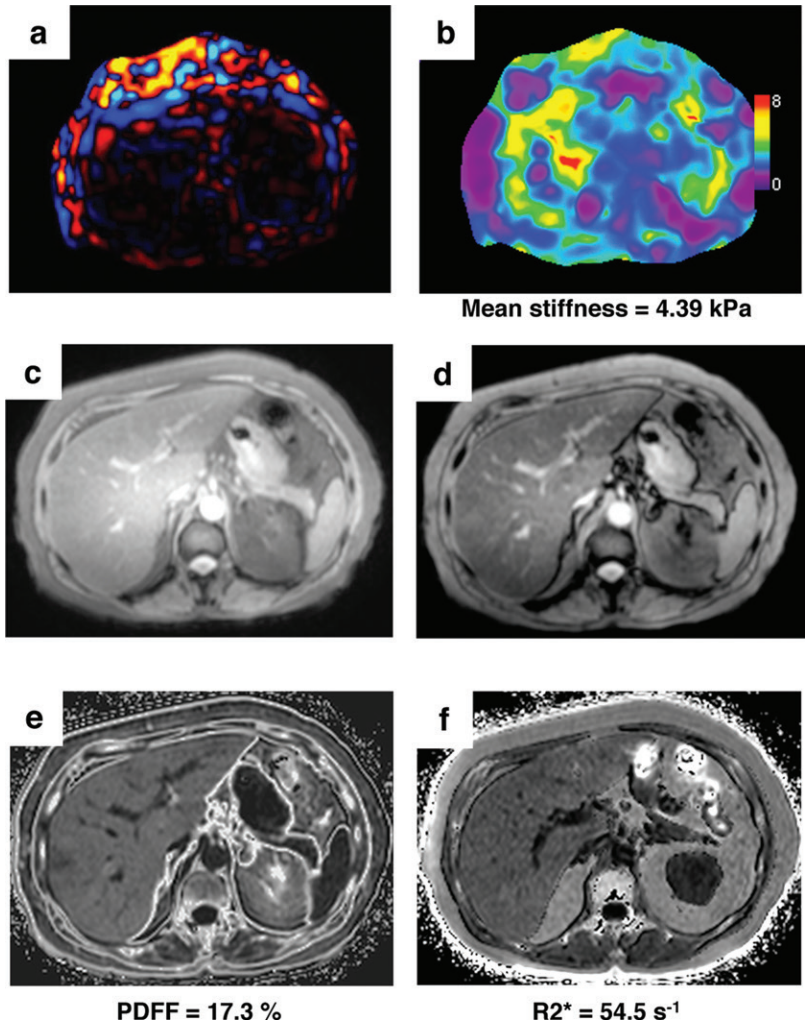

Figure 15. Biomarkers of chronic liver disease in a 65-year-old woman with biopsy-proved nonalcoholic steatohepatitis. Assessment was performed with multiparametric MR imaging at 3.0 T. *(a)* Wave image from elastography. *(b)* Elastogram shows liver stiffness of 4.39 kPa as a biomarker of liver fibrosis. *(c, d)* In-phase *(c)* and out-of-phase *(d)* images show signal drop on the out-of-phase image, indicative of liver steatosis. *(e)* Image shows a proton-density fat fraction *(PDFF)* of 17.3% as a biomarker of liver steatosis. *(f)* R2* map shows an R2* of 54.5 sec^{-1} as a biomarker of liver iron concentration. Liver biopsy demonstrated stage 2 fibrosis, grade 1 steatosis, and grade 0 iron concentration.

fibrosis (77) and multiecho chemical shift–encoded GRE sequences for simultaneous assessment of proton-density fat fraction (PDFF) for liver steatosis quantification and R2* for liver iron quantification within a single breath hold (Fig 15) (22,66,78). Proton-density fat fraction is a biomarker that has been validated for accurate and precise assessment of liver steatosis across different systems (79,80). Ultimately, combining several parameters may improve classification accuracy and lead to better diagnostic performance than use of single parameters (81,82).

Conclusion

Iron overload potentially leads to end-organ damage, with higher prevalence of liver (cirrhosis, hepatocellular carcinoma), endocrine, and cardiac complications. Therefore, detection and quantification of liver iron overload are critical to initiate treatment and prevent complications in hereditary hemochromatosis and transfusional hemosiderosis. Various MR imaging techniques, each with their respective advantages and limitations, have been developed for liver iron quantification. Because of the noninvasiveness and accuracy of these techniques, MR imaging–based liver iron quantification has become part of the standard of care in diagnosis and monitoring of iron overload diseases. In the near future, multiparametric quantitative protocols will permit simultaneous assessment of liver iron overload, as well as coexistent fat and fibrosis.

References

1. Brissot P, Loréal O. Iron metabolism and related genetic diseases: a cleared land, keeping mysteries. J Hepatol 2016;64(2):505–515.
2. Hernando D, Levin YS, Sirlin CB, Reeder SB. Quantification of liver iron with MRI: state of the art and remaining challenges. J Magn Reson Imaging 2014;40(5):1003–1021.
3. Wish JB. Assessing iron status: beyond serum ferritin and transferrin saturation. Clin J Am Soc Nephrol 2006;1(suppl 1):S4–S8.
4. McLaren CE, McLachlan GJ, Halliday JW, et al. Distribution of transferrin saturation in an Australian population: relevance to the early diagnosis of hemochromatosis. Gastroenterology 1998;114(3):543–549.
5. Esposito BP, Breuer W, Sirankapracha P, Pootrakul P, Hershko C, Cabantchik ZI. Labile plasma iron in iron overload: redox activity and susceptibility to chelation. Blood 2003;102(7):2670–2677.

6. Ohnishi S, Hara M, Furuno T, Sasabe H. Imaging the ordered arrays of water-soluble protein ferritin with the atomic force microscope. Biophys J 1992;63(5):1425–1431.
7. Pietrangelo A. Hereditary hemochromatosis: a new look at an old disease. N Engl J Med 2004;350(23):2383–2397.
8. Gattermann N. The treatment of secondary hemochromatosis. Dtsch Arztebl Int 2009;106(30):499–504, I.
9. Vlachos A, Ball S, Dahl N, et al. Diagnosing and treating Diamond Blackfan anaemia: results of an international clinical consensus conference. Br J Haematol 2008;142(6):859–876.
10. Modell B, Darlison M. Global epidemiology of haemoglobin disorders and derived service indicators. Bull World Health Organ 2008;86(6):480–487.
11. Flint J, Harding RM, Boyce AJ, Clegg JB. The population genetics of the haemoglobinopathies. Baillieres Clin Haematol 1998;11(1):1–51.
12. Li CK. New trend in the epidemiology of thalassaemia. Best Pract Res Clin Obstet Gynaecol 2017;39:16–26.
13. Kwan T, Leber B, Ahuja S, Carter R, Gerstein HC. Patients with type 2 diabetes have a high frequency of the C282Y mutation of the hemochromatosis gene. Clin Invest Med 1998;21(6):251–257.
14. Olivieri NF, Brittenham GM. Iron-chelating therapy and the treatment of thalassemia. Blood 1997;89(3):739–761.
15. Wood JC. Guidelines for quantifying iron overload. Hematology (Am Soc Hematol Educ Program) 2014;2014(1):210–215.
16. Sirlin CB, Reeder SB. Magnetic resonance imaging quantification of liver iron. Magn Reson Imaging Clin N Am 2010;18(3):359–381, ix.
17. Scheuer PJ, Williams R, Muir AR. Hepatic pathology in relatives of patients with haemochromatosis. J Pathol Bacteriol 1962;84:53–64.
18. Deugnier Y, Turlin B. Pathology of hepatic iron overload. World J Gastroenterol 2007;13(35):4755–4760.
19. Bedossa P, Carrat F. Liver fibrosis: screening is not staging. J Hepatol 2009;50(6):1268–1269.
20. Rockey DC, Caldwell SH, Goodman ZD, Nelson RC, Smith AD; American Association for the Study of Liver Diseases. Liver biopsy. Hepatology 2009;49(3):1017–1044.
21. St Pierre TG, Clark PR, Chua-anusorn W, et al. Noninvasive measurement and imaging of liver iron concentrations using proton magnetic resonance. Blood 2005;105(2):855–861.
22. França M, Alberich-Bayarri Á, Martí-Bonmatí L, et al. Accurate simultaneous quantification of liver steatosis and iron overload in diffuse liver diseases with MRI. Abdom Radiol (NY) 2017;42(5):1434–1443.
23. Emond MJ, Bronner MP, Carlson TH, Lin M, Labbe RF, Kowdley KV. Quantitative study of the variability of hepatic iron concentrations. Clin Chem 1999;45(3):340–346.
24. Wood JC, Zhang P, Rienhoff H, Abi-Saab W, Neufeld EJ. Liver MRI is more precise than liver biopsy for assessing total body iron balance: a comparison of MRI relaxometry with simulated liver biopsy results. Magn Reson Imaging 2015;33(6):761–767.
25. Eisenberg E, Konopniki M, Veitsman E, Kramskay R, Gaitini D, Baruch Y. Prevalence and characteristics of pain induced by percutaneous liver biopsy. Anesth Analg 2003;96(5):1392–1396, table of contents.
26. Lee YA, Wallace MC, Friedman SL. Pathobiology of liver fibrosis: a translational success story. Gut 2015;64(5):830–841. [Published correction appears in Gut 2015;64(8):1337.]
27. Hoffbrand AV, Taher A, Cappellini MD. How I treat transfusional iron overload. Blood 2012;120(18):3657–3669.
28. Porter J, Galanello R, Saglio G, et al. Relative response of patients with myelodysplastic syndromes and other transfusion-dependent anaemias to deferasirox (ICL670): a 1-yr prospective study. Eur J Haematol 2008;80(2):168–176.
29. Adams PC, Barton JC. How I treat hemochromatosis. Blood 2010;116(3):317–325.
30. Hankins JS, McCarville MB, Loeffler RB, et al. R2* magnetic resonance imaging of the liver in patients with iron overload. Blood 2009;113(20):4853–4855.
31. Rees DC, Williams TN, Gladwin MT. Sickle-cell disease. Lancet 2010;376(9757):2018–2031.
32. Qian Q, Nath KA, Wu Y, Daoud TM, Sethi S. Hemolysis and acute kidney failure. Am J Kidney Dis 2010;56(4):780–784.
33. Schein A, Enriquez C, Coates TD, Wood JC. Magnetic resonance detection of kidney iron deposition in sickle cell disease: a marker of chronic hemolysis. J Magn Reson Imaging 2008;28(3):698–704.
34. Noetzli LJ, Panigrahy A, Mittelman SD, et al. Pituitary iron and volume predict hypogonadism in transfusional iron overload. Am J Hematol 2012;87(2):167–171.
35. Berdoukas V, Nord A, Carson S, et al. Tissue iron evaluation in chronically transfused children shows significant levels of iron loading at a very young age. Am J Hematol 2013;88(11):E283–E285.
36. Brittenham GM, Badman DG; National Institute of Diabetes and Digestive and Kidney Diseases (NIDDK) Workshop. Noninvasive measurement of iron: report of an NIDDK workshop. Blood 2003;101(1):15–19.
37. Serai SD, Fleck RJ, Quinn CT, Zhang B, Podberesky DJ. Retrospective comparison of gradient recalled echo R2* and spin-echo R2 magnetic resonance analysis methods for estimating liver iron content in children and adolescents. Pediatr Radiol 2015;45(11):1629–1634.
38. Gandon Y, Olivié D, Guyader D, et al. Non-invasive assessment of hepatic iron stores by MRI. Lancet 2004;363(9406):357–362.
39. Paisant A, Boulic A, Bardou-Jacquet E, et al. Assessment of liver iron overload by 3 T MRI. Abdom Radiol (NY) 2017;42(6):1713–1720.
40. Olynyk JK, Luxon BA, Britton RS, Bacon BR. Hepatic iron concentration in hereditary hemochromatosis does not saturate or accurately predict phlebotomy requirements. Am J Gastroenterol 1998;93(3):346–350.
41. Adams PC. Factors affecting the rate of iron mobilization during venesection therapy for genetic hemochromatosis. Am J Hematol 1998;58(1):16–19.
42. Phatak PD, Barton JC. Phlebotomy-mobilized iron as a surrogate for liver iron content in hemochromatosis patients. Hematology 2003;8(6):429–432.
43. Olynyk JK, St Pierre TG, Britton RS, Brunt EM, Bacon BR. Duration of hepatic iron exposure increases the risk of significant fibrosis in hereditary hemochromatosis: a new role for magnetic resonance imaging. Am J Gastroenterol 2005;100(4):837–841.
44. Wood JC. Use of magnetic resonance imaging to monitor iron overload. Hematol Oncol Clin North Am 2014;28(4):747–764, vii.
45. Brittenham GM, Cohen AR, McLaren CE, et al. Hepatic iron stores and plasma ferritin concentration in patients with sickle cell anemia and thalassemia major. Am J Hematol 1993;42(1):81–85.
46. Belhoul KM, Bakir ML, Saned MS, Kadhim AM, Musallam KM, Taher AT. Serum ferritin levels and endocrinopathy in medically treated patients with β thalassemia major. Ann Hematol 2012;91(7):1107–1114.
47. Chapman RW, Hussain MA, Gorman A, et al. Effect of ascorbic acid deficiency on serum ferritin concentration in patients with beta-thalassaemia major and iron overload. J Clin Pathol 1982;35(5):487–491.
48. Cazzola M, Malcovati L. Diagnosis and treatment of sideroblastic anemias: from defective heme synthesis to abnormal RNA splicing. Hematology (Am Soc Hematol Educ Program) 2015;2015:19–25.
49. Koperdanova M, Cullis JO. Interpreting raised serum ferritin levels. BMJ 2015;351:h3692.
50. Lipschitz DA, Cook JD, Finch CA. A clinical evaluation of serum ferritin as an index of iron stores. N Engl J Med 1974;290(22):1213–1216.
51. Boll DT, Merkle EM. Diffuse liver disease: strategies for hepatic CT and MR imaging. RadioGraphics 2009;29(6):1591–1614.
52. Kojima S, Kojima S, Ueno H, Takeya M, Ogawa H. Increased density of the liver and amiodarone-associated phospholipidosis. Cardiol Res Pract 2009;2009:598940.
53. Yeh BM, Shepherd JA, Wang ZJ, Teh HS, Hartman RP, Prevrhal S. Dual-energy and low-kVp CT in the abdomen. AJR Am J Roentgenol 2009;193(1):47–54.
54. Karçaaltıncaba M, Aktas A. Dual-energy CT revisited with multidetector CT: review of principles and clinical applications. Diagn Interv Radiol 2011;17(3):181–194.
55. Rose C, Vandevenne P, Bourgeois E, Cambier N, Ernst O. Liver iron content assessment by routine and simple magnetic

resonance imaging procedure in highly transfused patients. Eur J Haematol 2006;77(2):145–149.
56. Hashemi RH. T1, T2, and T2*. In: MRI: the basics. 2nd ed. Philadelphia, Pa: Wolters Kluwer, 2010; 41–43.
57. Hashemi RH. Artefacts in MRI. In: MRI: the basics. 2nd ed. Philadelphia, Pa: Wolters Kluwer, 2010; 206–207.
58. Wood JC, Enriquez C, Ghugre N, et al. MRI R2 and R2* mapping accurately estimates hepatic iron concentration in transfusion-dependent thalassemia and sickle cell disease patients. Blood 2005;106(4):1460–1465.
59. Sharma SD, Fischer R, Schoennagel BP, et al. MRI-based quantitative susceptibility mapping (QSM) and R2* mapping of liver iron overload: comparison with SQUID-based biomagnetic liver susceptometry. Magn Reson Med 2017;78(1):264–270.
60. Runge JH, Akkerman EM, Troelstra MA, Nederveen AJ, Beuers U, Stoker J. Comparison of clinical MRI liver iron content measurements using signal intensity ratios, R2 and R2*. Abdom Radiol (NY) 2016;41(11):2123–2131.
61. Gandon Y. On-line liver iron quantification. https://imagemed.univ-rennes1.fr/en/mrquantif/online_quantif.php. Updated September 2017. Accessed January 13, 2018.
62. Gossuin Y, Roch A, Muller RN, Gillis P, Lo Bue F. Anomalous nuclear magnetic relaxation of aqueous solutions of ferritin: an unprecedented first-order mechanism. Magn Reson Med 2002;48(6):959–964.
63. Jensen JH, Chandra R. Theory of nonexponential NMR signal decay in liver with iron overload or superparamagnetic iron oxide particles. Magn Reson Med 2002;47(6):1131–1138.
64. Health R. FerriScan: MRI measurement of liver iron concentration. http://www.resonancehealth.com/products/ferriscan-mri-measurement-of-liver-iron-concentration.html. Accessed June 1, 2016.
65. Clark PR, Chua-anusorn W, St Pierre TG. Bi-exponential proton transverse relaxation rate (R2) image analysis using RF field intensity-weighted spin density projection: potential for R2 measurement of iron-loaded liver. Magn Reson Imaging 2003;21(5):519–530.
66. Horng DE, Hernando D, Reeder SB. Quantification of liver fat in the presence of iron overload. J Magn Reson Imaging 2017;45(2):428–439.
67. McCarville MB, Hillenbrand CM, Loeffler RB, et al. Comparison of whole liver and small region-of-interest measurements of MRI liver R2* in children with iron overload. Pediatr Radiol 2010;40(8):1360–1367.
68. Garbowski MW, Carpenter JP, Smith G, et al. Biopsy-based calibration of T2* magnetic resonance for estimation of liver iron concentration and comparison with R2 Ferriscan. J Cardiovasc Magn Reson 2014;16:40.
69. Yokoo T, Browning JD. Fat and iron quantification in the liver: past, present, and future. Top Magn Reson Imaging 2014;23(2):73–94.
70. Wang Y, Liu T. Quantitative susceptibility mapping (QSM): decoding MRI data for a tissue magnetic biomarker. Magn Reson Med 2015;73(1):82–101.
71. Sharma SD, Hernando D, Horng DE, Reeder SB. Quantitative susceptibility mapping in the abdomen as an imaging biomarker of hepatic iron overload. Magn Reson Med 2015;74(3):673–683.
72. Powell LW, Seckington RC, Deugnier Y. Haemochromatosis. Lancet 2016;388(10045):706–716.
73. Hanson EH, Imperatore G, Burke W. HFE gene and hereditary hemochromatosis: a HuGE review. Human Genome Epidemiology. Am J Epidemiol 2001;154(3):193–206.
74. Hunt JR, Zito CA, Johnson LK. Body iron excretion by healthy men and women. Am J Clin Nutr 2009;89(6):1792–1798.
75. Borgna-Pignatti C, Cappellini MD, De Stefano P, et al. Cardiac morbidity and mortality in deferoxamine- or deferiprone-treated patients with thalassemia major. Blood 2006;107(9):3733–3737.
76. Krafft AJ, Loeffler RB, Song R, et al. Quantitative ultrashort echo time imaging for assessment of massive iron overload at 1.5 and 3 Tesla. Magn Reson Med 2017;78(5):1839–1851.
77. Petitclerc L, Sebastiani G, Gilbert G, Cloutier G, Tang A. Liver fibrosis: review of current imaging and MRI quantification techniques. J Magn Reson Imaging 2017;45(5):1276–1295.
78. Reeder SB, Bice EK, Yu H, Hernando D, Pineda AR. On the performance of T2* correction methods for quantification of hepatic fat content. Magn Reson Med 2012;67(2):389–404.
79. Yokoo T, Shiehmorteza M, Hamilton G, et al. Estimation of hepatic proton-density fat fraction by using MR imaging at 3.0 T. Radiology 2011;258(3):749–759.
80. Tang A, Desai A, Hamilton G, et al. Accuracy of MR imaging–estimated proton density fat fraction for classification of dichotomized histologic steatosis grades in nonalcoholic fatty liver disease. Radiology 2015;274(2):416–425.
81. Feier D, Balassy C, Bastati N, Fragner R, Wrba F, Ba-Ssalamah A. The diagnostic efficacy of quantitative liver MR imaging with diffusion-weighted, SWI, and hepato-specific contrast-enhanced sequences in staging liver fibrosis: a multiparametric approach. Eur Radiol 2016;26(2):539–546.
82. Banerjee R, Pavlides M, Tunnicliffe EM, et al. Multiparametric magnetic resonance for the non-invasive diagnosis of liver disease. J Hepatol 2014;60(1):69–77.